 doi:10.20944/preprints202211.0025.v1

Article

Tectonothermal Events Revealed by Zircon U-Pb Dating of the Cretaceous Sandstones of Jingbian, Shaanxi and Their Origin

Hao Shi, Dapeng Yue *, Jingbo Zhao, Rong Liu, Xiaoning Wang, Yan Zhao and Le Liu

School of Geography and Tourism, Shaanxi Normal University, Xi'an, 710119; shihaosnnu@ qq. Com;(H.S)
* Correspondence: yuedp@ snnu. edu. Cn(D.P.Y)

Abstract: The Danxia landform area of Jingbian Wave Valley is located in the central part of Ordos Basin. The near-red Danxia landform consisting of sandstone in this area is a new discovery in geological circles at home and abroad, and its depositional age and genesis remain a hot topic of discussion at present. As the material basis for its development, red sandstone is of great importance to the in-depth study on its formation date and origin. The paper explores the origin, tectonic significance and paleogeographic pattern of the red sandstone through field geological investigation and zircon U-Pb dating analysis of the red sandstone of the Luohe Formation. The results show that the original materials of the red sandstone was formed in three main age intervals, 252~456 Ma, 1657~2084 Ma, and 2129~2538 Ma, and regional tectonothermal events in the origin area during the three periods were recorded, among which the events in Mesoproterozoic and Paleoproterozoic periods were the most active. The comparative analysis of zircon U-Pb age spectra shows that for the sediment of red sandstone, the early origin is near-origin and late origin is distant-origin. The main origin areas in the study area are the Xingmeng orogenic belt, the North China massif and the Alashan massif; the vertical section reflects that the origin area has the strongest erosion and transport in the upper deposition period, the smallest erosion and transport in the middle deposition period, and the moderate erosion and transport in the lower deposition period. With origins system dominated by the northern origins and the paleogeographic pattern of multi-period and cyclonic, the area mainly experienced four tectonic movement cycles, such as Wutai, Lvliang, Caledon and Haixi.

Keywords: Ordos Basin; red sandstone; detrital zircon U-Pb dating; tectonothermal events; origin analysis; Danxia landform area in northern Shaanxi; China

1. Introduction

As a type of landform characterized by steep cliff slopes with the red bed as the material base[1], Danxia Landform is distributed in many places around the world. Most of the Danxia landforms in China evolved from the development of the Mesozoic Cretaceous-dominated red beds, which are mainly concentrated in the southwest, southeast and northwest regions[2]; red beds and Danxia landforms abroad are widely exposed in Europe [3]and North America [4-6]. The Danxia landform exposed in northern Shaanxi, China, is a new discovery and a continuous focus of geological circles at home and abroad in recent years[7,8]. A huge thick red bed is buried under the Quaternary loess and a rare wave-like Danxia landform feature is developed on this red bed, together with the discovery of dinosaur footprints[9]. Therefore, it boasts high landscape value, tourism development potential and scientific value. The tectonic environment, material basis, and landform features of the formation period of this red bed differ significantly from the Danxia landforms in southeastern China, but it shares many similarities with the Danxia landforms in the western United States[10,11]. Under different geographical environments and geological and tectonic conditions, the rock properties of the red bed and the landform morphology of its development can show significant regional differences, leading to

 doi:10.20944/preprints202211.0025.v1

many controversies on scientific issues such as morphological characteristics, development conditions, and evolutionary processes of the Danxia landforms. In general, past studies on the Danxia landform area focused on macroscopic descriptions and discussions, instead of exploring the sedimentary rock characteristics, sandstone clastic composition, sedimentary environment analysis and the nature of the origin of the red bed in the area. As the material basis for the development of the Danxia landform, red sandstone records the information of the origin and the depositional area in material components, which is an inevitable issue in the study of the Danxia landform. Zircon, as the most common and stable heavy mineral in sediments, is of great interest to study. Fedo et al [12]suggested that zircon has a high U-Pb isotope system closure temperature, which is little affected by sedimentation and diagenesis, and can play a key role in origin analysis. XU Huan [13], WANG Yujia[14], YANG Qingkun[15] , et al. carried out Zircon U-Pb dating analyses in the red bed sandstone of the Danxia Basin in Fujian, Jiangxi, and Guangdong, China, and obtained new insights into the tectonic setting, physical origin, and paleoclimatic features of the region. Safonova I et al [16] and Shuang Li et al [17] carried out U-Pb dating analyses of sandstone sediments to determine the origins, depositional age and tectonic setting in eastern Kazakhstan and Ramando area in southwest Indonesia respectively. Weltje and Eynatten [18]; Andersen [19]qualified the nature of the sediment origin, depositional environment and depositional age by the U-Pb chronology of detrital zircons, and determined that zircon chronology studies are an important tool to investigate the formation of the basin and the tectonic evolution of its origin. In this paper, we propose to use LA-ICP-MS method on the basis of field geological investigation to perform U-Pb dating of detrital zircons from red sandstone in the Jingbian wavy Danxia landform. By analyzing the chronological data, combining the mineralogical component characteristics and some previous research results, the paper explores the origin characteristics, paleogeographic pattern and tectonic background of the output, and trace the depositional process of the origin and provides important sedimentological information for the in-depth study of the genesis of red sandstone, the formation era and the development mechanism of wavy Danxia landform. Meanwhile, it also provides some scientific basis for the further study of the scientific value of red bed Danxia in northern Shaanxi and the development and utilization of Danxia landform area.

2. Overview of study area

Jingbian Danxia Landform Distribution Area in northern Shaanxi is located near Longzhou Town, about 22km southeast of Jingbian County, with geographical coordinates of 108°59'30″—109°00'35″ east longitude and 37°30'35″—37°31'50″ north latitude, in the transition zone between Loess Plateau and Mu Us Sandy Land in northern Shaanxi.

In terms of geotectonic units, the Jingbian area belongs to the northern Shaanxi slope in the central part of the Ordos Basin with Tianhuan depression in the west, Jinxi flexural fold belt in the east, Weibei uplift in the south, and Yimeng uplift in the north (Figures 1a, 1b). The Ordos Basin is a large inland depressional basin developed on the basis of the North China Craton Platform [20]. Before the Mesozoic, the area was in the stage of ancient crystalline basement formation and Paleozoic cover deposition, and after the formation of the Ordos land mass, its main body was in the epicontinental near-sea plain environment for a long time. Under the influence of seawater erosion and ebb, the terrestrial red bed was rarely accumulated. In the Triassic, affected by Indochinese movement, the margin of Ordos land mass began to uplift, and the central area in the study area steadily subsided and entered the development period of inland basin, when the depositional environment completely changed into continental system. The paleoclimate was hot and arid and the area began to receive successive deposits of terrestrial red clastic rocks. By the Early Cretaceous, the Yanshan movement caused the uplift of Lvliang Mountains in the eastern part of the study area, further depression of the Ordos land mass, and complete separation from the North China Plateau, forming the independent Ordos Basin, showing a paleomorphological pattern of low in the west and high in the east[21]. During this period, the

Preprints (www.preprints.org) | NOT PEER-REVIEWED | Posted: 1 November 2022 doi:10.20944/preprints202211.0025.v1

paleoclimate changed to a warm and humid subtropical climate, and rivers and lakes developed, with huge thick red clastic rocks of the Cretaceous Zhidan Group accumulated, which is the material basis for the formation of Danxia landforms in the later period. In the Late Cretaceous, the Ordos Basin began to uplift as a whole, and the study area turned into an exfoliated environment. Since the Cenozoic, affected by complex intermittent tectonic uplift by the Himalayan and Neotectonic movements, Paleoproterozoic and Neoproterozoic strata were absent and a series of joints and fractures formed, which provided important conditions for the development of wavy Danxia landforms in the area.

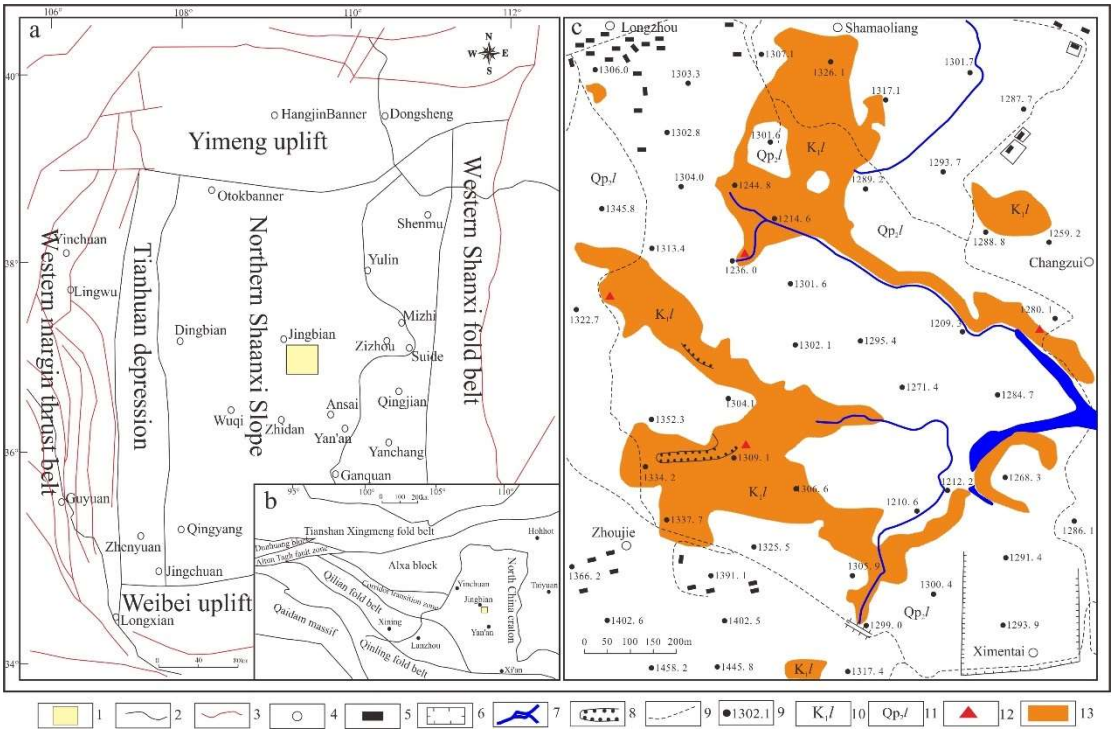

Figure 1. Ordos Basin Regional Tectonic Unit (a)[22], Geotectonic location (b), and Distribution sketch of Danxia landform red sandstone in Jingbian Wave-liked Valley (c). 1-Research area; 2-Fault; 3-Construction zone line; 4-place name; 5-House; 6-Slab wall; 7-Rivers; 8-Canyon; 9-Road; 10-Altimetric point; 11-Luohe formation of Zhidan group of Cretaceous system; 11-Quaternary Middle Pleistocene; 12-Sample point; 13-Red sandstone.

On the basis of red sandstone material, unique landforms with diverse morphology and ornamental value were developed, which became important tourism resources and have now been established as China National Geopark tourist attractions (Figure 1c). The area is also known as the wavy Danxia landform because of its rounded, smooth, wave-like features and micro-formations such as “gyroscopic”, “oil tower” and “ribbon-like” (Figure 2).

The field geological investigation shows that the sandstone of the Luohe Formation of the Cretaceous Zhidan Group exposed in the study area is in unconformable contact with the upper Quaternary loess, and is mainly a set of river-lake phase assemblage in sedimentary phase, with red, reddish-brown and reddish-white colors. They are mainly fine-medium sandstone, partly medium-coarse sandstone, with poor sortability, medium roundness, and mineral composition dominated by plagioclase, potassium feldspar and quartz (Figure 2).

 doi:10.20944/preprints202211.0025.v1

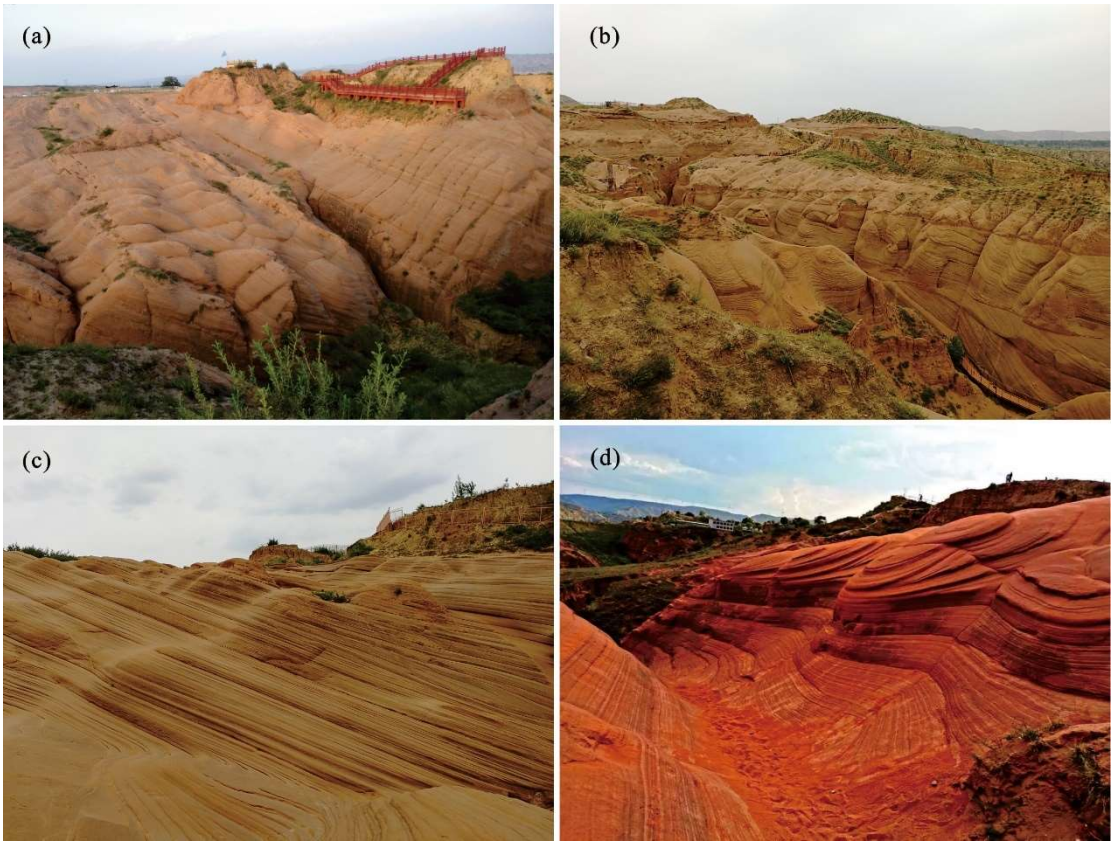

Figure 2. Morphological characteristics of Danxia landform red sandstone in Jingbian Wave-liked Valley.

3. Sample collection and analysis methods

In this study, three red sandstone samples were collected from the upper (LZ-1), middle (LZ-2) and lower (LZ-3) parts of the Danxia landform area in Jingbian, Shaanxi Province, based on the field geological survey, with the weight of each sample being about 5 kg. The sampling locations are shown in Figure 1c. The three dated rock samples collected in the field were mechanically crushed to about 60 mesh by conventional methods, and the heavy minerals were sorted out by conventional gravity flotation and electromagnetic methods, before the representative zircon grains (good crystal shape and transparency, no cleavage) were hand-selected under a binocular microscope for determination. The selected zircon particles were then subjected to the preparation of zircon sample targets. After the zircon targets were prepared, cathodoluminescence (CL) imaging observations were performed to determine the internal structure of the zircon particles and the zircon particles and locations suitable for analysis for LA-MC-ICP-MS determination. Cathodoluminescence image studies were done on a HITACHI S3000-N scanning electron microscope equipped with a GATAN Chroma cathodoluminescence probe analytical instrument. The LA- MC-ICP-MS zircon U-Pb age test was performed on a ThermoFinningan Neptune multi-receiver plasma mass spectrometer. The detailed analytical procedure, experimental principles and instrument parameters were described by HOU Kejun et al[23], and the calculation program Isoplot (version 3.0) [24], developed by Kenneth R. Ludwig, Berkeley Center for Geological Dating, USA, was used for the processing harmony and plotting of the age data. Common Pb and age corrections performed on the samples were calculated using the Anderson method [25], and U-Pb harmonic plots were completed using the Isoplot program[24].

In this study, the U-Pb ages of 191 detrital zircons were randomly selected and tested from three red sandstone samples. Based on the influence of radioactive Pb isotopes, in this paper, for the specific age analysis, the surface age of $^{207}Pb/^{206}Pb$ was used for zircons

 doi:10.20944/preprints202211.0025.v1

with $^{206}Pb/^{238}U$ age > 1000 Ma, and for zircons with $^{206}Pb/^{238}U$ age < 1000 Ma, zircons were analyzed using $^{206}Pb/^{238}U$ surface ages, while for zircons<500Made, $^{206}Pb/^{238}U$ age values were also used since Pb was not lost. Data with harmonics between 90% and 100% are considered valid [26-29]. The above experimental procedure was carried out at Beijing Gaonian Linghang Technology Co., Ltd.

4. Experimental results and analysis

4.1. Zircon characteristics and genesis

The U, Th, and Pb contents, Th/U ratios, and U-Pb surface ages of detrital zircons in red sandstone LZ-1, LZ-2, and LZ-3 at each measurement point are detailed in Table 1. Cathodoluminescence photographs of representative zircon grains are shown in Figure 3, and the zircon U-Pb age harmonic curves and age histograms are shown in Figure 4.

Table 1. Detrital zircon U-Pb dating results of the red sandstone.

Number	Contents/ppm				Isotope Ratios						U-Pb Age/Ma					
	Pb	Th	U	Th/U	$^{207}Pb/^{235}U$	2σ	$^{206}Pb/^{238}U$	2σ	$^{207}Pb/^{206}Pb$	2σ	$^{207}Pb/^{235}U$	2σ	$^{206}Pb/^{238}U$	2σ	$^{207}Pb/^{206}Pb$	2σ
LZ-1 - 1	206.8	206.8	534.0	0.39	5.3900	0.1400	0.3443	0.0084	0.1127	0.0026	1882	22.0	1907	40.0	1840	41.0
LZ-1 - 2	53.6	39.4	107.7	0.37	7.2900	0.2000	0.4001	0.0074	0.1296	0.0031	2144	24.0	2169	34.0	2084	43.0
LZ-1 - 3	162.6	189.3	419.6	0.45	4.4800	0.1300	0.3116	0.0058	0.1021	0.0030	1727	24.0	1748	28.0	1657	54.0
LZ-1 - 4	29.5	47.3	68.9	0.69	5.2700	0.1200	0.3367	0.0053	0.1127	0.0022	1859	20.0	1870	26.0	1826	37.0
LZ-1 - 5	112.9	124.3	184.1	0.68	9.8300	0.2800	0.4533	0.0088	0.1542	0.0036	2417	27.0	2410	39.0	2389	40.0
LZ-1 - 6	146.5	147.7	400.2	0.37	4.8100	0.1200	0.3136	0.0062	0.1130	0.0027	1786	22.0	1758	30.0	1844	43.0
LZ-1 - 7	57.1	49.0	143.6	0.34	5.1100	0.1200	0.3275	0.0058	0.1113	0.0025	1836	20.0	1826	28.0	1812	40.0
LZ-1 - 8	227.4	208.1	535.1	0.39	5.5640	0.0900	0.3461	0.0049	0.1157	0.0012	1909	14.0	1916	23.0	1888	18.0
LZ-1 - 9	4.5	51.5	88.2	0.58	0.3200	0.0390	0.0445	0.0014	0.0514	0.0065	277	30.0	281	8.5	150	240.0
LZ-1 - 10	82.6	48.9	166.0	0.29	7.9700	0.2100	0.4112	0.0072	0.1391	0.0025	2218	26.0	2219	33.0	2205	33.0
LZ-1 - 11	3.5	34.5	66.6	0.52	0.3260	0.0250	0.0449	0.0010	0.0526	0.0039	280	19.0	282	5.9	180	150.0
LZ-1 - 12	182.1	239.5	349.9	0.68	7.8490	0.1300	0.4117	0.0063	0.1382	0.0014	2213	14.0	2222	29.0	2202	18.0
LZ-1 - 13	165.9	57.1	325.9	0.18	8.4800	0.1800	0.4276	0.0070	0.1412	0.0023	2282	20.0	2294	31.0	2238	28.0
LZ-1 - 14	1.8	20.6	33.0	0.62	0.3230	0.0380	0.0438	0.0013	0.0549	0.0066	268	30.0	276	7.8	90	230.0
LZ-1 - 15	180.5	48.4	458.0	0.11	5.6080	0.0990	0.3472	0.0057	0.1181	0.0014	1916	15.0	1921	27.0	1923	22.0
LZ-1 - 16	86.1	36.3	150.1	0.24	11.4100	0.3100	0.4918	0.0091	0.1684	0.0034	2555	25.0	2578	40.0	2538	34.0
LZ-1 - 17	89.6	61.7	219.4	0.28	5.8100	0.1200	0.3558	0.0062	0.1204	0.0022	1947	18.0	1962	29.0	1957	33.0
LZ-1 - 18	70.0	78.4	160.7	0.49	5.8110	0.0980	0.3549	0.0052	0.1186	0.0015	1947	15.0	1957	25.0	1928	23.0
LZ-1 - 19	46.0	73.7	94.5	0.78	5.9300	0.1900	0.3615	0.0067	0.1173	0.0036	1961	28.0	1989	32.0	1902	54.0
LZ-1 - 20	158.3	157.0	398.0	0.39	5.7100	0.1500	0.3517	0.0062	0.1158	0.0018	1930	23.0	1943	29.0	1889	28.0
LZ-1 - 21	21.8	45.5	47.5	0.96	5.2000	0.1800	0.3356	0.0079	0.1122	0.0034	1849	28.0	1863	38.0	1831	55.0
LZ-1 - 23	23.3	28.9	61.4	0.47	4.5100	0.2100	0.3026	0.0065	0.1061	0.0048	1726	39.0	1704	32.0	1708	87.0
LZ-1 - 24	94.0	118.1	384.3	0.31	2.3010	0.0570	0.2094	0.0033	0.0790	0.0017	1211	18.0	1225	18.0	1169	21.0
LZ-1 - 25	50.9	88.4	122.0	0.72	4.9300	0.0980	0.3230	0.0049	0.1104	0.0017	1804	17.0	1804	24.0	1806	26.0
LZ-1 - 26	67.6	213.1	121.5	1.75	5.5600	0.1700	0.3456	0.0059	0.1165	0.0033	1906	27.0	1913	28.0	1892	52.0
LZ-1 - 27	77.8	133.8	181.6	0.74	5.2470	0.0910	0.3336	0.0048	0.1138	0.0016	1858	15.0	1855	23.0	1853	25.0
LZ-1 - 28	122.5	40.3	298.8	0.13	5.6900	0.1500	0.3536	0.0072	0.1152	0.0029	1933	21.0	1951	34.0	1875	45.0
LZ-1 - 29	19.3	28.4	43.4	0.66	5.6600	0.1600	0.3518	0.0062	0.1176	0.0030	1925	25.0	1942	30.0	1911	43.0
LZ-1 - 30	4.4	67.9	73.0	0.93	0.3390	0.0250	0.0463	0.0010	0.0531	0.0038	292	20.0	291	6.2	220	150.0
LZ-1 - 31	22.2	43.7	55.0	0.79	4.5900	0.1200	0.3092	0.0051	0.1075	0.0025	1740	21.0	1736	25.0	1739	42.0
LZ-1 - 32	164.4	108.4	281.5	0.39	10.7170	0.1400	0.4723	0.0064	0.1642	0.0013	2498	12.0	2493	28.0	2498	13.0
LZ-1 - 33	60.0	151.5	313.8	0.48	1.5990	0.0320	0.1625	0.0023	0.0713	0.0012	968	12.0	970	13.0	956	33.0
LZ-1 - 34	46.5	61.6	67.7	0.91	11.2400	0.2900	0.4877	0.0093	0.1662	0.0037	2544	25.0	2560	40.0	2511	37.0
LZ-1 - 36	5.2	73.3	78.2	0.94	0.3880	0.0240	0.0516	0.0010	0.0547	0.0036	330	17.0	324	6.4	280	130.0
LZ-1 - 37	139.7	227.3	220.4	1.03	10.6200	0.2200	0.4736	0.0081	0.1625	0.0023	2489	19.0	2499	35.0	2479	24.0
LZ-1 - 38	11.8	15.4	30.2	0.51	5.2700	0.2000	0.3358	0.0074	0.1126	0.0045	1858	33.0	1866	36.0	1839	68.0
LZ-1 - 39	185.6	342.6	488.0	0.70	4.3330	0.0690	0.3009	0.0043	0.1045	0.0010	1698	13.0	1696	21.0	1702	18.0
LZ-1 - 40	201.3	235.3	463.1	0.51	5.4950	0.0910	0.3450	0.0050	0.1147	0.0015	1899	14.0	1913	22.0	1871	23.0
LZ-1 - 41	110.7	109.9	259.9	0.42	5.4900	0.1000	0.3436	0.0058	0.1143	0.0015	1898	16.0	1904	28.0	1865	24.0
LZ-1 - 42	113.7	87.4	256.6	0.34	6.0400	0.1900	0.3626	0.0075	0.1193	0.0035	1980	26.0	1994	35.0	1938	53.0
LZ-1 - 43	53.2	46.1	106.7	0.43	7.9300	0.2100	0.4118	0.0071	0.1381	0.0020	2215	23.0	2225	33.0	2201	26.0
LZ-1 - 44	143.2	30.9	353.7	0.09	6.5840	0.1200	0.3793	0.0066	0.1268	0.0016	2056	15.0	2073	31.0	2055	21.0
LZ-1 - 45	24.7	50.2	42.9	1.17	8.3200	0.3100	0.4150	0.0100	0.1482	0.0050	2261	34.0	2236	47.0	2313	58.0

 doi:10.20944/preprints202211.0025.v1

LZ-1 - 46	45.1	111.3	160.2	0.69	2.5740	0.0530	0.2242	0.0033	0.0835	0.0014	1292	15.0	1304	17.0	1275	33.0
LZ-1 - 47	3.9	58.8	80.0	0.74	0.2860	0.0210	0.0398	0.0008	0.0526	0.0040	252	17.0	252	5.2	220	150.0
LZ-1 - 48	13.5	66.4	273.2	0.24	0.3160	0.0120	0.0451	0.0007	0.0507	0.0019	277	9.5	285	4.6	188	77.0
LZ-1 - 49	16.3	37.2	34.9	1.07	5.3800	0.1400	0.3383	0.0058	0.1148	0.0028	1876	23.0	1877	28.0	1874	45.0
LZ-1 - 50	47.7	100.1	105.2	0.95	5.2320	0.1000	0.3363	0.0049	0.1132	0.0016	1854	17.0	1868	24.0	1845	26.0
LZ-1 - 51	7.6	59.8	82.2	0.73	0.5580	0.0310	0.0734	0.0015	0.0550	0.0029	446	20.0	456	8.8	360	110.0
LZ-1 - 52	81.5	61.0	204.0	0.30	5.7560	0.1100	0.3535	0.0051	0.1155	0.0014	1936	17.0	1951	24.0	1886	23.0
LZ-1 - 53	127.8	34.8	363.3	0.10	4.9850	0.0850	0.3240	0.0050	0.1125	0.0014	1816	14.0	1809	24.0	1836	22.0
LZ-1 - 54	190.9	23.5	327.4	0.07	11.4400	0.2900	0.4906	0.0110	0.1683	0.0031	2558	24.0	2573	47.0	2538	30.0
LZ-1 - 55	53.9	68.0	81.0	0.84	10.3300	0.3100	0.4732	0.0097	0.1568	0.0045	2462	28.0	2496	43.0	2412	48.0
LZ-1 - 56	2.7	53.8	44.9	1.20	0.3060	0.0300	0.0435	0.0012	0.0520	0.0054	261	23.0	275	7.3	90	190.0
LZ-1 - 57	59.2	87.6	87.7	1.00	11.2000	0.2100	0.4820	0.0076	0.1691	0.0024	2536	17.0	2535	33.0	2547	23.0
LZ-1 - 58	132.2	181.8	338.7	0.54	5.2300	0.1200	0.3362	0.0063	0.1113	0.0015	1856	20.0	1868	30.0	1818	24.0
LZ-1 - 59	105.5	275.2	197.4	1.39	5.8520	0.0970	0.3563	0.0053	0.1195	0.0013	1953	14.0	1964	25.0	1948	21.0
LZ-1 - 60	5.4	14.1	13.6	1.03	3.9700	0.2000	0.2938	0.0067	0.0989	0.0049	1603	42.0	1658	33.0	1500	30.0
LZ-1 - 61	89.8	100.9	168.9	0.60	7.8500	0.1200	0.4139	0.0060	0.1380	0.0015	2215	14.0	2232	27.0	2197	19.0
LZ-1 - 62	140.9	121.1	262.7	0.46	8.6900	0.1300	0.4321	0.0061	0.1463	0.0013	2305	13.0	2315	28.0	2300	16.0
LZ-1 - 63	23.8	17.4	42.4	0.41	9.9700	0.2300	0.4538	0.0073	0.1600	0.0030	2425	21.0	2411	32.0	2442	32.0

LZ-2 - 1	113.8	85.5	211.7	0.40	9.9100	0.2800	0.4621	0.0097	0.1538	0.0035	2425	25.0	2448	43.0	2384	38.0
LZ-2 - 2	115.8	165.0	178.3	0.93	11.7700	0.3800	0.4976	0.0093	0.1664	0.0028	2582	30.0	2603	40.0	2518	28.0
LZ-2 - 3	6.0	75.7	110.6	0.68	0.3140	0.0200	0.0442	0.0010	0.0518	0.0033	273	15.0	279	5.9	180	130.0
LZ-2 - 4	82.5	125.3	170.2	0.74	5.7570	0.1200	0.3521	0.0051	0.1190	0.0017	1936	17.0	1944	25.0	1931	26.0
LZ-2 - 5	117.6	225.4	263.2	0.86	5.5640	0.0970	0.3448	0.0055	0.1179	0.0013	1909	15.0	1910	27.0	1922	20.0
LZ-2 - 6	112.0	116.5	241.9	0.48	6.1900	0.2100	0.3695	0.0088	0.1216	0.0034	2001	29.0	2027	41.0	1974	51.0
LZ-2 - 7	49.2	59.3	76.6	0.77	10.7600	0.2000	0.4775	0.0070	0.1644	0.0023	2501	17.0	2516	31.0	2494	24.0
LZ-2 - 8	145.1	202.0	246.3	0.82	8.9600	0.1800	0.4389	0.0078	0.1511	0.0024	2333	19.0	2345	35.0	2356	28.0
LZ-2 - 9	42.6	77.3	100.1	0.77	5.1500	0.1300	0.3341	0.0059	0.1129	0.0024	1841	22.0	1858	28.0	1834	39.0
LZ-2 - 10	25.6	52.5	56.0	0.94	5.2400	0.1100	0.3363	0.0053	0.1137	0.0022	1857	18.0	1868	26.0	1847	35.0
LZ-2 - 11	74.3	142.9	133.0	1.07	7.3800	0.1500	0.3946	0.0069	0.1361	0.0025	2156	18.0	2144	32.0	2171	32.0
LZ-2 - 12	88.1	130.2	196.7	0.66	5.3600	0.1300	0.3416	0.0058	0.1135	0.0024	1877	21.0	1894	28.0	1849	39.0
LZ-2 - 13	88.4	185.3	183.4	1.01	5.3100	0.1600	0.3403	0.0063	0.1123	0.0027	1868	25.0	1888	30.0	1829	45.0
LZ-2 - 14	36.0	38.7	66.5	0.58	8.5600	0.2300	0.4305	0.0078	0.1469	0.0035	2288	24.0	2307	35.0	2300	42.0
LZ-2 - 15	201.9	225.0	491.0	0.46	5.8100	0.1200	0.3560	0.0066	0.1181	0.0020	1948	18.0	1963	31.0	1925	30.0
LZ-2 - 16	34.4	46.4	83.9	0.55	5.1160	0.1100	0.3288	0.0049	0.1136	0.0020	1838	18.0	1832	24.0	1844	33.0
LZ-2 - 17	200.2	159.5	411.5	0.39	7.9600	0.1600	0.4169	0.0073	0.1386	0.0023	2225	18.0	2246	33.0	2206	28.0
LZ-2 - 18	21.9	29.6	50.0	0.59	5.6700	0.1700	0.3541	0.0065	0.1176	0.0035	1920	26.0	1953	31.0	1896	54.0
LZ-2 - 19	39.9	54.3	61.5	0.88	10.7200	0.2300	0.4762	0.0076	0.1644	0.0027	2495	20.0	2510	33.0	2493	27.0
LZ-2 - 20	91.0	94.2	167.8	0.56	8.9900	0.2300	0.4457	0.0089	0.1460	0.0029	2334	23.0	2375	40.0	2295	35.0
LZ-2 - 21	68.1	44.7	126.7	0.35	8.4200	0.1900	0.4250	0.0068	0.1430	0.0027	2274	20.0	2283	31.0	2256	33.0
LZ-2 - 22	268.4	112.3	690.0	0.16	5.9100	0.1200	0.3561	0.0086	0.1169	0.0010	1959	17.0	1960	41.0	1906	15.0
LZ-2 - 23	58.9	84.3	100.1	0.84	8.5700	0.2000	0.4302	0.0074	0.1447	0.0027	2291	21.0	2306	33.0	2278	32.0
LZ-2 - 24	431.8	515.9	920.0	0.56	6.1640	0.0880	0.3651	0.0059	0.1222	0.0011	1999	13.0	2006	28.0	1988	15.0
LZ-2 - 25	97.5	79.6	157.0	0.51	11.2200	0.1900	0.4838	0.0075	0.1679	0.0021	2540	16.0	2543	33.0	2533	21.0
LZ-2 - 26	117.4	65.5	276.6	0.24	6.0500	0.1600	0.3553	0.0081	0.1246	0.0025	1982	23.0	1960	39.0	2021	35.0
LZ-2 - 27	5.9	61.9	113.9	0.54	0.3020	0.0170	0.0435	0.0008	0.0507	0.0030	265	14.0	274	4.8	170	120.0
LZ-2 - 28	92.6	5.5	225.1	0.02	6.0900	0.2300	0.3544	0.0089	0.1238	0.0047	1987	34.0	1955	42.0	2003	65.0
LZ-2 - 29	48.9	51.1	91.3	0.56	8.2600	0.1600	0.4217	0.0067	0.1429	0.0020	2257	17.0	2267	30.0	2256	24.0
LZ-2 - 30	86.8	177.2	176.5	1.00	5.5370	0.1000	0.3468	0.0054	0.1152	0.0020	1905	16.0	1919	26.0	1877	31.0
LZ-2 - 31	35.9	30.9	77.6	0.40	6.4700	0.1400	0.3761	0.0060	0.1252	0.0023	2037	19.0	2062	30.0	2019	33.0
LZ-2 - 32	30.9	48.2	71.8	0.67	5.4100	0.1600	0.3445	0.0056	0.1144	0.0027	1881	24.0	1908	27.0	1865	44.0
LZ-2 - 33	111.7	72.6	271.5	0.27	6.2030	0.1200	0.3689	0.0063	0.1208	0.0016	2006	18.0	2024	30.0	1965	24.0
LZ-2 - 34	128.0	143.8	300.0	0.48	6.0500	0.1600	0.3660	0.0087	0.1197	0.0026	1982	24.0	2010	41.0	1948	38.0
LZ-2 - 35	18.2	8.0	44.1	0.18	6.0300	0.1300	0.3594	0.0060	0.1218	0.0023	1977	18.0	1978	29.0	1972	33.0
LZ-2 - 36	134.0	142.1	260.3	0.55	7.7000	0.1100	0.4086	0.0059	0.1367	0.0013	2195	13.0	2208	27.0	2182	16.0
LZ-2 - 37	79.9	102.0	196.0	0.52	5.0000	0.1700	0.3223	0.0073	0.1109	0.0029	1816	30.0	1800	35.0	1807	48.0
LZ-2 - 39	14.4	12.7	36.3	0.35	5.4400	0.2500	0.3473	0.0070	0.1137	0.0049	1878	40.0	1921	34.0	1823	78.0
LZ-2 - 40	301.5	233.9	777.0	0.30	5.3640	0.0980	0.3382	0.0063	0.1152	0.0008	1877	16.0	1877	30.0	1880	13.0
LZ-2 - 41	91.8	61.4	220.3	0.28	5.4500	0.1400	0.3411	0.0078	0.1144	0.0025	1890	22.0	1891	37.0	1864	39.0
LZ-2 - 42	38.3	93.1	80.0	1.16	4.9900	0.1700	0.3303	0.0064	0.1084	0.0038	1812	29.0	1839	31.0	1755	64.0
LZ-2 - 43	43.7	44.4	71.2	0.62	10.7500	0.2400	0.4783	0.0092	0.1630	0.0028	2499	20.0	2519	40.0	2482	30.0
LZ-2 - 44	116.6	141.0	172.1	0.82	11.1700	0.2000	0.4811	0.0072	0.1673	0.0022	2536	17.0	2531	31.0	2527	22.0
LZ-2 - 45	13.4	81.4	153.3	0.53	0.5700	0.0210	0.0730	0.0012	0.0569	0.0021	455	14.0	455	6.8	429	79.0
LZ-2 - 46	172.2	199.2	427.6	0.47	5.5300	0.1700	0.3440	0.0055	0.1122	0.0011	1900	24.0	1905	26.0	1831	18.0

 doi:10.20944/preprints202211.0025.v1

LZ-2 - 47	66.1	85.6	118.1	0.72	8.4400	0.1900	0.4249	0.0072	0.1438	0.0019	2273	20.0	2281	32.0	2266	23.0
LZ-2 - 48	154.9	72.9	272.0	0.27	10.5710	0.1400	0.4697	0.0066	0.1632	0.0013	2485	13.0	2482	29.0	2486	13.0
LZ-2 - 49	224.9	153.8	481.6	0.32	6.6300	0.1400	0.3786	0.0065	0.1256	0.0020	2062	19.0	2069	30.0	2033	29.0
LZ-2 - 50	6.6	72.5	73.5	0.99	0.5070	0.0460	0.0654	0.0018	0.0566	0.0052	407	31.0	408	11.0	330	190.0
LZ-2 - 51	81.8	137.8	139.0	0.99	8.5800	0.1800	0.4284	0.0077	0.1457	0.0019	2291	19.0	2301	36.0	2290	22.0
LZ-2 - 52	19.1	34.6	36.7	0.94	6.6700	0.2300	0.3732	0.0071	0.1285	0.0038	2059	30.0	2043	34.0	2063	56.0
LZ-2 - 53	123.7	154.9	191.9	0.81	10.0100	0.2100	0.4623	0.0076	0.1550	0.0023	2433	20.0	2449	33.0	2398	26.0
LZ-2 - 54	47.7	44.0	121.9	0.36	5.4600	0.1700	0.3449	0.0074	0.1143	0.0027	1892	27.0	1909	35.0	1862	43.0
LZ-2 - 55	193.5	237.2	432.4	0.55	6.1980	0.0970	0.3648	0.0060	0.1238	0.0013	2003	14.0	2004	28.0	2007	18.0
LZ-2 - 56	27.6	40.7	66.7	0.61	5.2100	0.1500	0.3374	0.0060	0.1126	0.0032	1848	26.0	1873	29.0	1824	54.0
LZ-2 - 57	328.3	82.2	866.0	0.09	5.5500	0.1300	0.3465	0.0084	0.1171	0.0009	1905	20.0	1916	40.0	1911	14.0
LZ-2 - 58	3.0	32.2	56.9	0.57	0.2920	0.0260	0.0438	0.0010	0.0487	0.0043	255	21.0	277	6.0	30	170.0
LZ-2 - 59	70.6	93.7	115.5	0.81	9.7600	0.1700	0.4520	0.0066	0.1565	0.0020	2411	16.0	2403	29.0	2412	22.0
LZ-2 - 60	99.5	60.0	240.4	0.25	5.5600	0.1100	0.3473	0.0052	0.1150	0.0019	1908	17.0	1921	25.0	1878	29.0

LZ-4 - 1	78.4	85.9	116.4	0.74	11.3300	0.2100	0.5068	0.0084	0.1619	0.0020	2547	18.0	2641	36.0	2469	21.0
LZ-4 - 2	8.2	63.8	160.1	0.40	0.3190	0.0180	0.0459	0.0009	0.0512	0.0029	278	14.0	289	5.5	190	120.0
LZ-4 - 4	4.5	49.2	83.5	0.59	0.3420	0.0290	0.0461	0.0012	0.0544	0.0048	294	22.0	291	7.6	280	180.0
LZ-4 - 5	247.1	292.3	473.2	0.62	7.8610	0.1100	0.4092	0.0056	0.1389	0.0010	2214	12.0	2211	25.0	2212	12.0
LZ-4 - 6	39.4	88.9	104.4	0.85	3.9620	0.0950	0.2834	0.0046	0.1010	0.0021	1623	20.0	1608	23.0	1636	38.0
LZ-4 - 7	217.2	133.0	378.2	0.35	11.1500	0.1800	0.4857	0.0073	0.1670	0.0016	2535	15.0	2551	32.0	2525	17.0
LZ-4 - 8	209.4	225.9	321.5	0.70	10.7800	0.2300	0.4803	0.0085	0.1615	0.0033	2503	20.0	2528	37.0	2469	34.0
LZ-4 - 9	33.0	160.6	716.0	0.22	0.3047	0.0090	0.0430	0.0008	0.0513	0.0012	269	6.9	272	4.7	234	53.0
LZ-4 - 10	243.9	270.0	437.3	0.62	8.4340	0.1300	0.4260	0.0063	0.1421	0.0014	2278	14.0	2287	28.0	2251	17.0
LZ-4 - 11	56.4	37.9	108.1	0.35	8.4200	0.2000	0.4170	0.0076	0.1444	0.0030	2274	22.0	2246	35.0	2273	35.0
LZ-4 - 12	43.6	37.7	86.1	0.44	8.4100	0.2300	0.4199	0.0078	0.1441	0.0024	2267	24.0	2258	35.0	2265	29.0
LZ-4 - 13	58.5	32.8	144.2	0.23	5.7590	0.1100	0.3482	0.0053	0.1205	0.0017	1940	16.0	1925	25.0	1957	25.0
LZ-4 - 14	6.9	4.7	16.7	0.28	5.9700	0.2500	0.3552	0.0069	0.1206	0.0047	1954	36.0	1958	33.0	1920	71.0
LZ-4 - 15	78.0	103.6	187.1	0.55	5.0400	0.1500	0.3335	0.0061	0.1094	0.0025	1824	24.0	1855	29.0	1782	42.0
LZ-4 - 16	195.5	173.9	381.5	0.46	7.7400	0.1400	0.4112	0.0064	0.1365	0.0019	2200	17.0	2220	29.0	2179	24.0
LZ-4 - 17	132.8	88.6	223.3	0.40	11.3400	0.1800	0.4861	0.0076	0.1683	0.0016	2551	14.0	2555	32.0	2537	16.0
LZ-4 - 18	80.0	63.9	188.8	0.34	5.6300	0.1300	0.3520	0.0058	0.1144	0.0021	1920	20.0	1944	28.0	1865	34.0
LZ-4 - 19	164.5	179.2	335.6	0.53	7.7300	0.2000	0.4120	0.0063	0.1325	0.0013	2196	22.0	2223	29.0	2129	17.0
LZ-4 - 20	9.3	125.7	158.1	0.80	0.3340	0.0170	0.0471	0.0009	0.0512	0.0025	289	13.0	297	5.5	186	96.0
LZ-4 - 21	37.5	26.4	83.5	0.32	7.2300	0.2000	0.3987	0.0076	0.1268	0.0030	2136	25.0	2162	35.0	2049	40.0
LZ-4 - 22	261.1	140.8	626.0	0.22	5.8690	0.0910	0.3552	0.0052	0.1203	0.0013	1957	14.0	1959	25.0	1957	19.0
LZ-4 - 23	84.5	71.3	203.7	0.35	5.4650	0.1100	0.3453	0.0057	0.1136	0.0019	1893	17.0	1912	27.0	1852	31.0
LZ-4 - 24	80.8	60.3	213.3	0.28	5.2900	0.1100	0.3386	0.0055	0.1133	0.0018	1865	17.0	1880	26.0	1848	28.0
LZ-4 - 25	89.9	39.3	238.4	0.16	5.1570	0.0830	0.3340	0.0050	0.1114	0.0013	1843	14.0	1857	24.0	1816	20.0
LZ-4 - 26	188.1	149.5	440.4	0.34	6.1610	0.1000	0.3650	0.0051	0.1216	0.0012	1998	14.0	2006	24.0	1975	18.0
LZ-4 - 27	100.5	108.9	174.4	0.62	9.5100	0.1500	0.4512	0.0064	0.1518	0.0015	2386	14.0	2400	28.0	2362	17.0
LZ-4 - 29	12.3	168.6	237.3	0.71	0.2910	0.0130	0.0421	0.0007	0.0502	0.0022	259	10.0	266	4.3	155	89.0
LZ-4 - 30	33.6	392.0	476.0	0.82	0.4083	0.0110	0.0550	0.0008	0.0538	0.0014	347	7.8	345	5.1	339	56.0
LZ-4 - 31	70.6	117.7	135.7	0.87	6.7100	0.1500	0.3798	0.0059	0.1266	0.0025	2071	20.0	2075	28.0	2043	35.0
LZ-4 - 33	205.3	310.3	523.8	0.59	4.6000	0.0680	0.3108	0.0043	0.1067	0.0010	1748	12.0	1744	21.0	1742	17.0
LZ-4 - 34	107.4	60.6	280.0	0.22	5.6970	0.1100	0.3521	0.0055	0.1142	0.0012	1928	16.0	1944	26.0	1863	19.0
LZ-4 - 35	38.3	67.8	80.1	0.85	5.6600	0.1600	0.3523	0.0066	0.1151	0.0033	1921	24.0	1945	31.0	1868	52.0
LZ-4 - 36	106.3	185.1	168.2	1.10	10.3300	0.3000	0.4696	0.0078	0.1521	0.0016	2459	25.0	2481	34.0	2374	20.0
LZ-4 - 37	140.3	77.8	326.8	0.24	6.5820	0.1200	0.3794	0.0056	0.1227	0.0011	2055	16.0	2073	26.0	1992	16.0
LZ-4 - 38	78.7	137.0	191.0	0.72	5.3330	0.1100	0.3382	0.0050	0.1130	0.0015	1871	17.0	1880	25.0	1842	24.0
LZ-4 - 39	83.2	76.6	159.7	0.48	9.1800	0.2700	0.4436	0.0084	0.1493	0.0024	2354	27.0	2366	38.0	2335	28.0
LZ-4 - 40	186.7	158.6	431.0	0.37	5.8470	0.1000	0.3553	0.0056	0.1173	0.0017	1952	15.0	1960	27.0	1912	26.0
LZ-4 - 42	10.0	107.8	179.2	0.60	0.3090	0.0190	0.0443	0.0008	0.0503	0.0030	271	14.0	279	5.0	160	120.0
LZ-4 - 43	524.7	61.4	1370.0	0.04	5.5900	0.1500	0.3482	0.0092	0.1173	0.0016	1913	23.0	1925	44.0	1912	25.0
LZ-4 - 44	44.6	31.1	109.0	0.29	5.5100	0.1300	0.3454	0.0061	0.1144	0.0024	1898	21.0	1912	29.0	1859	39.0
LZ-4 - 45	67.0	77.2	161.5	0.48	5.8100	0.1300	0.3570	0.0055	0.1142	0.0015	1944	19.0	1967	26.0	1861	24.0
LZ-4 - 46	167.7	107.1	421.8	0.25	5.8070	0.1200	0.3536	0.0051	0.1157	0.0011	1947	17.0	1952	24.0	1887	17.0
LZ-4 - 47	20.8	24.0	40.6	0.59	7.4700	0.1900	0.3973	0.0072	0.1351	0.0031	2167	22.0	2156	33.0	2156	43.0
LZ-4 - 48	112.4	37.4	289.0	0.13	5.6580	0.1000	0.3510	0.0051	0.1147	0.0012	1926	16.0	1939	24.0	1870	20.0
LZ-4 - 49	334.0	11.2	890.0	0.01	5.7020	0.1100	0.3483	0.0065	0.1179	0.0008	1929	16.0	1925	31.0	1922	12.0
LZ-4 - 50	57.5	101.7	130.6	0.78	5.7200	0.1600	0.3530	0.0060	0.1169	0.0030	1932	24.0	1948	29.0	1901	45.0
LZ-4 - 51	158.8	123.8	273.6	0.45	10.1100	0.2200	0.4592	0.0081	0.1596	0.0027	2443	20.0	2435	36.0	2447	28.0
LZ-4 - 52	91.4	100.8	232.2	0.43	5.6000	0.1700	0.3480	0.0064	0.1123	0.0019	1912	26.0	1924	31.0	1832	30.0
LZ-4 - 53	119.5	60.7	324.1	0.19	5.2600	0.1200	0.3330	0.0066	0.1141	0.0014	1858	21.0	1852	32.0	1865	22.0

Preprints (www.preprints.org) | NOT PEER-REVIEWED | Posted: 1 November 2022 doi:10.20944/preprints202211.0025.v1

LZ-4 - 54	279.3	171.6	535.9	0.32	9.0000	0.1500	0.4389	0.0066	0.1479	0.0013	2336	15.0	2345	30.0	2319	15.0
LZ-4 - 55	16.2	40.1	78.9	0.51	1.6910	0.0490	0.1715	0.0028	0.0708	0.0021	1002	19.0	1020	15.0	925	60.0
LZ-4 - 56	45.5	140.8	91.9	1.53	5.3300	0.1600	0.3382	0.0057	0.1136	0.0028	1870	25.0	1882	29.0	1847	46.0
LZ-4 - 57	76.7	127.2	167.5	0.76	5.8050	0.0990	0.3540	0.0050	0.1167	0.0013	1944	15.0	1953	24.0	1903	19.0
LZ-4 - 58	81.1	74.0	142.0	0.52	10.0800	0.2500	0.4653	0.0077	0.1499	0.0019	2437	21.0	2462	34.0	2343	22.0
LZ-4 - 59	65.6	81.4	116.6	0.70	9.2500	0.1900	0.4456	0.0075	0.1503	0.0025	2361	19.0	2375	33.0	2345	28.0
LZ-4 - 60	11.1	26.5	24.1	1.10	5.0900	0.1600	0.3327	0.0065	0.1104	0.0033	1823	26.0	1850	31.0	1769	54.0
LZ-4 - 61	68.7	109.2	273.7	0.40	2.4850	0.0460	0.2138	0.0031	0.0836	0.0011	1265	13.0	1249	16.0	1275	26.0
LZ-4 - 62	138.0	122.8	244.6	0.50	9.0310	0.1300	0.4468	0.0065	0.1453	0.0013	2339	14.0	2383	30.0	2290	15.0
LZ-4 - 64	31.8	85.9	65.2	1.32	5.1500	0.1200	0.3327	0.0052	0.1104	0.0022	1839	19.0	1851	25.0	1802	39.0
LZ-4 - 66	147.7	104.7	339.2	0.31	6.2980	0.1100	0.3662	0.0058	0.1237	0.0012	2015	15.0	2011	27.0	2006	17.0
LZ-4 - 67	67.9	77.5	363.9	0.21	1.6630	0.0300	0.1674	0.0025	0.0714	0.0010	994	12.0	998	14.0	958	27.0
LZ-4 - 68	159.9	106.9	415.0	0.26	5.4980	0.0930	0.3345	0.0054	0.1178	0.0009	1898	14.0	1859	26.0	1919	14.0

CL images show (Figure 3) that zircon grain sizes vary widely, generally between 80-130 μm and individually up to 170μm. Microscopic observation shows that most of the zircon grains are colorless and transparent or light yellow, with more zircon intact crystalline form than fragmented grains, with rounding ranging from no rounding to better rounding. It's mainly rounded, sub-rounded and sub-angular, with fewer long columnar grains, reflecting that the material origin of the red sandstone is complex, and the transport distance varies greatly. Most of the grains have clear internal oscillatory rings and irregular zoning, with a good degree of automorphism, and some of them also have inclusions, indicating that their original genesis is magmatic zircon; a few of the grains have complex structures, with residual nuclei, and light bright white accretionary edges, either wide or narrow, with the characteristics of magmatic capture zircon or metamorphic zircon, which are products of late metamorphism; individual grains are darker in color, with no zoning or weak zoning structure. The internal structure is cloudy and complex, and the genesis is unknown, probably from ancient basement. The complex and diverse zircon morphology reflects the different types of zircon genesis, and also implies the complexity of the origin.

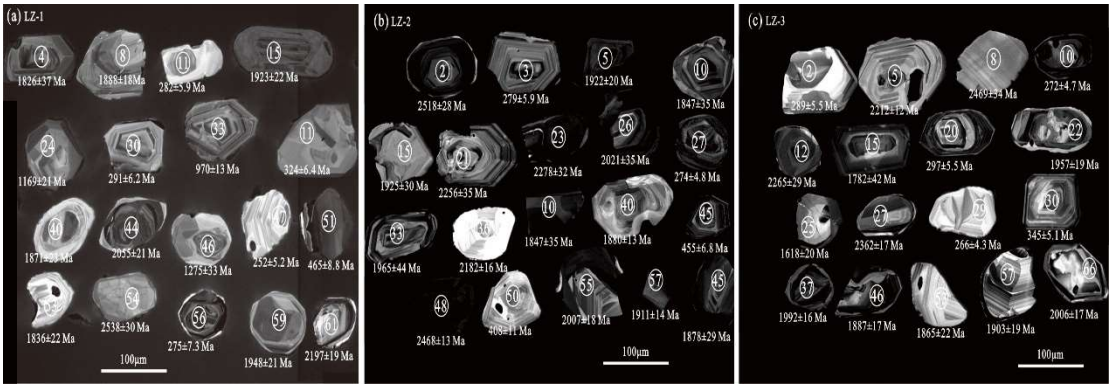

Figure 3. Representative Cathodoluminescence images of selected detrital zircon in red sandstone samples LZ-1(a), LZ-2(b) and LZ-3(3) in Danxia landform area of Jingbian.

The Th/U values of zircons can also reflect the type of zircon genesis; in general, magmatic zircons are relatively enriched in Th and U elements with Th/U > 0.4; metamorphic zircons are relatively low in Th and U elements with Th/U < 0.1[30,31]. Among the 182 data that met the harmonicity in this experiment, the Th content of zircon ranged from 4.7×10^{-6} to 515.9×10^{-6}, and the U content ranged from 13.6×10^{-6} to 1370.0×10^{-6}, with Th/U values ranging from 0.01 to 1.75 and an average value of 0.58. Among them, zircons with Th/U > 0.4 accounted for 67.03%, zircons with Th/U ratios between 0.1 and 0.4 accounted for 29.12%, and zircons with Th/U < 0.1 accounted for 3.85%. The Th/U ratio reveals that most of the zircons are of magmatic origin, some of them have undergone metamorphic accretion or less complete metamorphic recrystallization, and very few of them are of metamorphic origin.

 doi:10.20944/preprints202211.0025.v1

4.2. Zircon age distribution characteristics

A total of 61 valid zircon age data meeting the harmonicity requirement were obtained for the upper sandstone sample (LZ-1) of the red sandstone section in the study area. The overall distribution of zircon U-Pb ages ranges from 252 to 2547 Ma, and the age data are concentrated in three main age intervals: (1) 252-456 Ma age group, with 9 zircon grains, belongs to the Late Paleozoic, accounting for 14.75% of the total with the peak age of 284 Ma; (2) 1657-2084 Ma age group, with 32 zircon grains, belongs to the early to late Miocene, accounting for 52.46% of the total, with peak ages of 1869 Ma, 1916 Ma and 1955 Ma, respectively; (3) 2197-2538 Ma age group, with 16 zircon grains, belongs to the early to mid-Paleogene, accounting for 26.23% of the total, with peak ages of 2228 Ma and 2495 Ma. 4 other zircon grains are relatively scattered distributed in the early-Middle Neogene with U-Pb ages of 970±13 Ma, 1169±21 Ma, 1275±33 Ma, and 1500 ±30 Ma, respectively (Figures 4a, 4b).

A total of 59 valid zircon age data meeting the harmonicity requirement were obtained for the sandstone samples in the central part of the red sandstone section (LZ-2) in the study area. The overall distribution of zircon U-Pb ages ranges from 274 to 2518 Ma, and the age data are concentrated in three main age intervals: (1) 274-455 Ma age group, with 5 zircon grains, belongs to the Late Paleozoic, accounting for 8.47% of the total, with the peak age of 275 Ma; (2) 1755-2063 Ma age group, with 33 zircon grains, belongs to the middle and late Paleozoic, accounting for 55.94% of the total, with the peak age of 1911 Ma; (3) 2171-2533 Ma age group, with 21 zircon grains, belongs to the early and middle Paleozoic, accounting for 35.59% of the total, with the peak ages of 2293 Ma and 2524 Ma (Figures 4c, 4d).

A total of 62 valid zircon age data meeting the harmonicity requirement were obtained for the lower sandstone sample (LZ-3) of the red sandstone section in the study area. The overall distribution of zircon U-Pb ages ranges from 266 to 2537 Ma, and the age data are concentrated in three main age intervals: (1) 266-345 Ma age group, with 7 zircon grains, belongs to the Late Paleozoic, accounting for 11.29% of the total, with the peak age of 289 Ma; (2) 1742-2049 Ma age group, with 32 zircon grains, belongs to the middle to late Paleogene, accounting for 51.62% of the total, with peak ages of 1859 Ma and 1950 Ma; (3) 2129-2537 Ma age group, with 19 zircon grains, belongs to the early to middle Paleogene, accounting for 30.65% of the total, with peak ages of 2221 Ma, 2384 Ma and 2552 Ma. Another four zircons are relatively sporadically distributed in the early Neogene to late Miocene with U-Pb ages of 998±14 Ma, 1020±15 Ma, 1275±26 Ma, and 1636±38 Ma, respectively (Figures 4e, 4f).

Preprints (www.preprints.org) | NOT PEER-REVIEWED | Posted: 1 November 2022 doi:10.20944/preprints202211.0025.v1

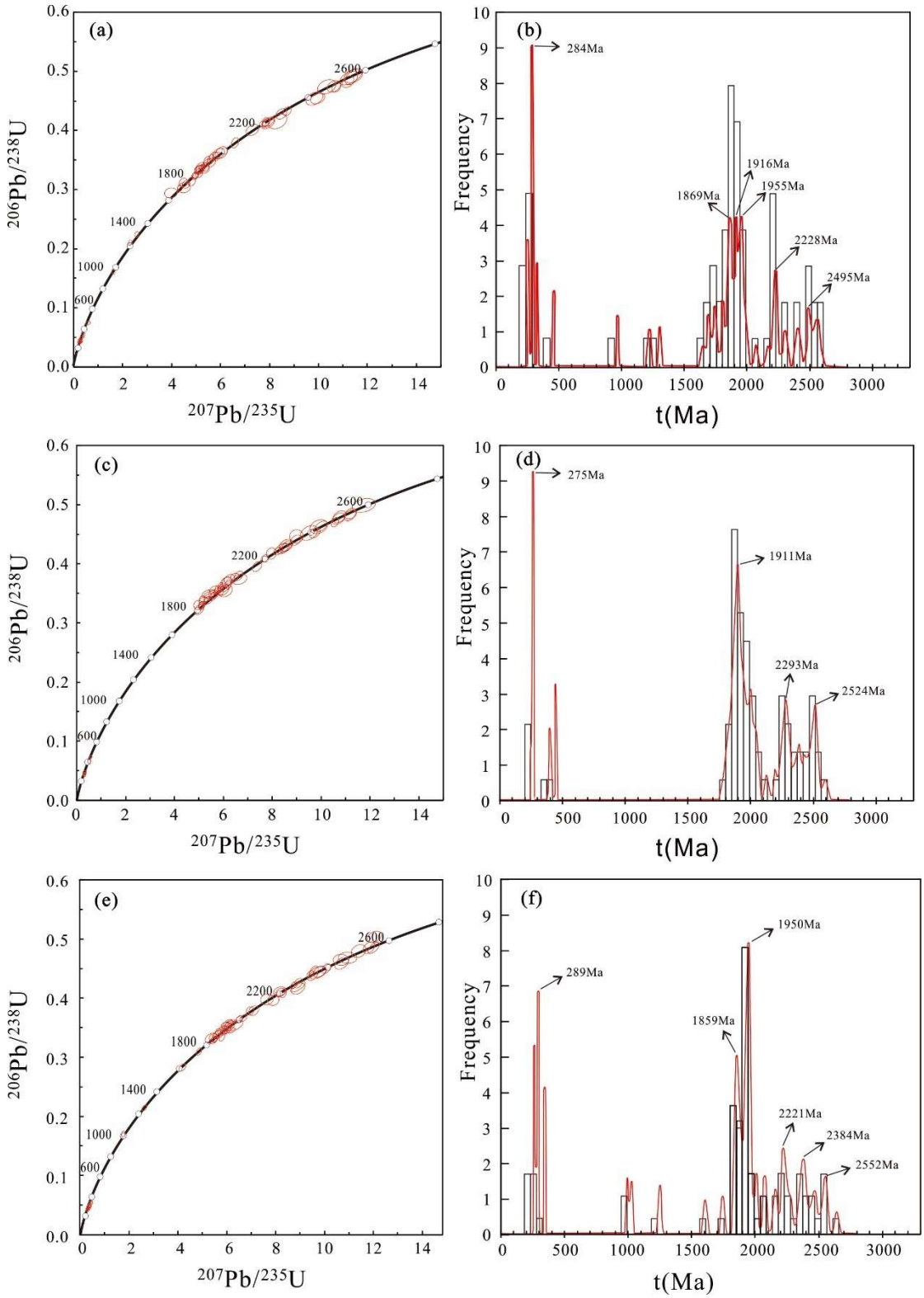

Figure 4. U-Pb Concordia diagrams and U-Pb age histograms for detrital zircons from red sandstone in Danxia landform area of Jingbian.

5. Discussion

5.1. Tectonothermal event and origin analysis

Since clastic materials from different origins have different age compositions, the zircon age distribution of the same sediments in the origin area shares similarity, while the

 doi:10.20944/preprints202211.0025.v1

zircon age spectra of different origin areas and distinctly different strata with different rock ages in the origin area are less similar, and the adjacent Qinling-Qilian orogenic belt, the Alashan massif, the Tianshan-Xingmeng orogenic belt, and the North China Craton platform in the study area may provide origin. By comparing and synthesizing the ages of outcrops in the neighboring areas around the perimeter of the basin with the zircon ages of the basins stratigraphic clasts, information on the origin of a stratum in the basin can be revealed[12,32].

Based on the comprehensive study and analysis of the dating results of the red sandstone samples from the upper (LZ-1), central (LZ-2) and lower (LZ-3) parts of the study area mentioned above, most of the 182 zircons with valid dating data obtained in this study are magmatic zircons, and three main age intervals (groups) can be identified on the age data histograms (Figures 4b, 4d, 4f), 252~456 Ma (Paleozoic), 1657~ 2084 Ma (Early Mesozoic-Late Paleozoic), and 2129-2538 Ma (Early-Middle Paleozoic), which record the regional tectonothermal events in the origin area or region that may be in three major periods. Among them, the Mesoproterozoic and Paleoproterozoic are the most prominent, implying that these two periods were more active in tectonic-magmatic activity and were the most important periods of tectonic activity in the region.

252~456 Ma: This interval has 21 sets of age data in three samples, accounting for about 11.54% of the total (182 zircons, the same below). The zircons have a clear rhythmic ring-band structure, which is typical of magmatic zircons, corresponding to the magmatic-tectonothermal event in Late Permian-Late Devonian Hesperian period and the tectonic magmatic event in Middle Ordovician-Late Silurian Garidon period. This part of the age spectra is more similar to the northern Xingmeng orogenic belt and the northern margin of the North China Craton (Figures 5e, 5f). Previous scholars[33,34] performed zircon U-Pb dating on clastic and metamorphic rocks in the Xingmeng orogenic belt and found that zircons with 250 Ma~350 Ma age were abundant. In contrast, the closure of the Solon suture zone between the northern margin of the North China plate and the southern margin of the Siberian plate was roughly 230 Ma~310 Ma[35], and it is speculated that during the closure process, a large amount of volcanic magma products exposed in the Xingmeng orogenic belt were denuded and transported with orogenic movements, providing the main origin for the study area. In addition, the North China Craton underwent a complex multi-stage tectonic evolutionary history, and the subduction, ablation, and collision of the Paleo-Asian Oceanic plate to the North China Massif during the Late Paleozoic-Early Mesozoic period[36] and the activity events of regional fractures on the North China margin may also provide some origin during this period.

1657~2084 Ma: This interval has 97 sets of age data in three samples, accounting for about 53.29% of the total. The zircon main body shows magmatic orogenic zircon, with a small proportion of metamorphic orogenic zircon, and the age spectra features of this part are more similar to those of the North Qilian orogenic belt, the Alashan massif, and the North China massif (Figure 5b, 5d, 5f). Some scholars suggested that intra-land orogeny occurred in the North China plate from 1900 to 2300 Ma[37], which recorded the evolution of the formation and closure of the North China Craton rift, with a granite zircon U-Pb age of 1958±34 Ma at the time of collision [38], and a potassium long granite U-Pb age of 2018±16 Ma in Longxian at the southwest margin of the North China plate[39]. The above reveals the possibility that the North China plate provided origin for the surrounding area in the Middle Ages. The Alashan massif, located in the northwestern part of the study area, has a similar rock composition and crustal evolution history as the North China Craton, and also developed Paleoproterozoic magmatic thermal events and two important metamorphic events from 1900 to 1950 Ma and 1800 to 1850 Ma[40], which coincide with the two tectonothermal events in the late Paleoproterozoic of the Kongzian belt at the northwestern margin of the North China Craton. Different study results indicate that the U-Pb age of the Bayan-Ula gneissic granodiorite in Alashan is 2080 Ma[41], the U-Pb age of the Kongzian system at the eastern margin of the Alashan Massif is 1900-1950 Ma [42], and

 doi:10.20944/preprints202211.0025.v1

the zircon LA-ICP-MS age results in the metamorphosed sedimentary rocks and granodioritic gneisses of the Longshushan Complex at the southern margin of Alashan also indicate that their formation is related to the Paleoproterozoic (2.01~2.17 Ga)[43]. In addition, some scholars[44,45] also concluded that 1982 Ma peak ages existed in the late Paleozoic of the North Qilian orogenic belt, and the possibility that the North Qilian orogenic belt provided a small amount of origins during that period cannot be excluded. In summary, the early Middle to late Paleozoic origin in the study area mainly originate from the North China Massif and the Alashan Massif.

2129~2538 Ma: This interval has 56 sets of age data in three samples, accounting for about 30.77% of the total. The zircon is mainly characterized by magmatic zircon with darker color, more turbid internal structure, and generally better rounding, reflecting the characteristics that ancient zircon has experienced multiple metamorphic events and multi-phase transport, and the age spectra characteristics of this part are more similar to those of the North China Massif and Alashan Massif (Figures 5d, 5f). Large-scale magmatic and metamorphic events occurred within the North China Platform during 2500 Ma, forming an ancient basement dominated by TTG gneisses and mantle-derived granites, marking the basic formation of the North China Craton [46,47]. Scholars'U-Pb dating results of detrital zircons from the Great Wall System cores of the Ordos Massif indicate the existence of 1950 Ma, 2350 Ma, 2500 Ma tectonic peak magma ages[47-49]. The Qilianshan basement rocks and the Longshan miscellaneous rocks distributed in the North Qilianshan Mountains record two magmatic events from 2350 to 2400 Ma and 2450 to 2500 Ma[50,51]. In contrast, the North Dashan rocks of the Alashan Massif also record a concordant age with 2496±11 Ma[52]and a peak age of 2329 Ma is recorded in the interior of the massif [53,54]. Zircon ages similar to the older ages in the detrital zircons of this interval are commonly present. In summary, the old basal crystalline facies of the North China plate and the multi-phase magmatic thermal events of the Alashan massif have good correspondence with the Paleozoic age of this study and provide origin for this age interval.

In addition, eight zircons sporadically distributed in the age interval of 970±13 Ma~1636±38 Ma correspond to the Grenville phase orogenic events, suggesting that they are related to the Grenville phase tectonic magmatism. However, the percentage is small, indicating that the origin area is not in the center of the Rodinia supercontinent, but probably in its peripheral area. The Mesozoic-Early Neoproterozoic magmatic thermal events occurred in the Erdos periphery area, and some data show that the Helanshan area can also provide Middle-Neoproterozoic zircons to the study area[55](Figure 5c), and based on the comparison of age spectra, the possibility that the Helanshan area provides a small amount of origins to the study area cannot be excluded.

Preprints (www.preprints.org) | NOT PEER-REVIEWED | Posted: 1 November 2022 doi:10.20944/preprints202211.0025.v1

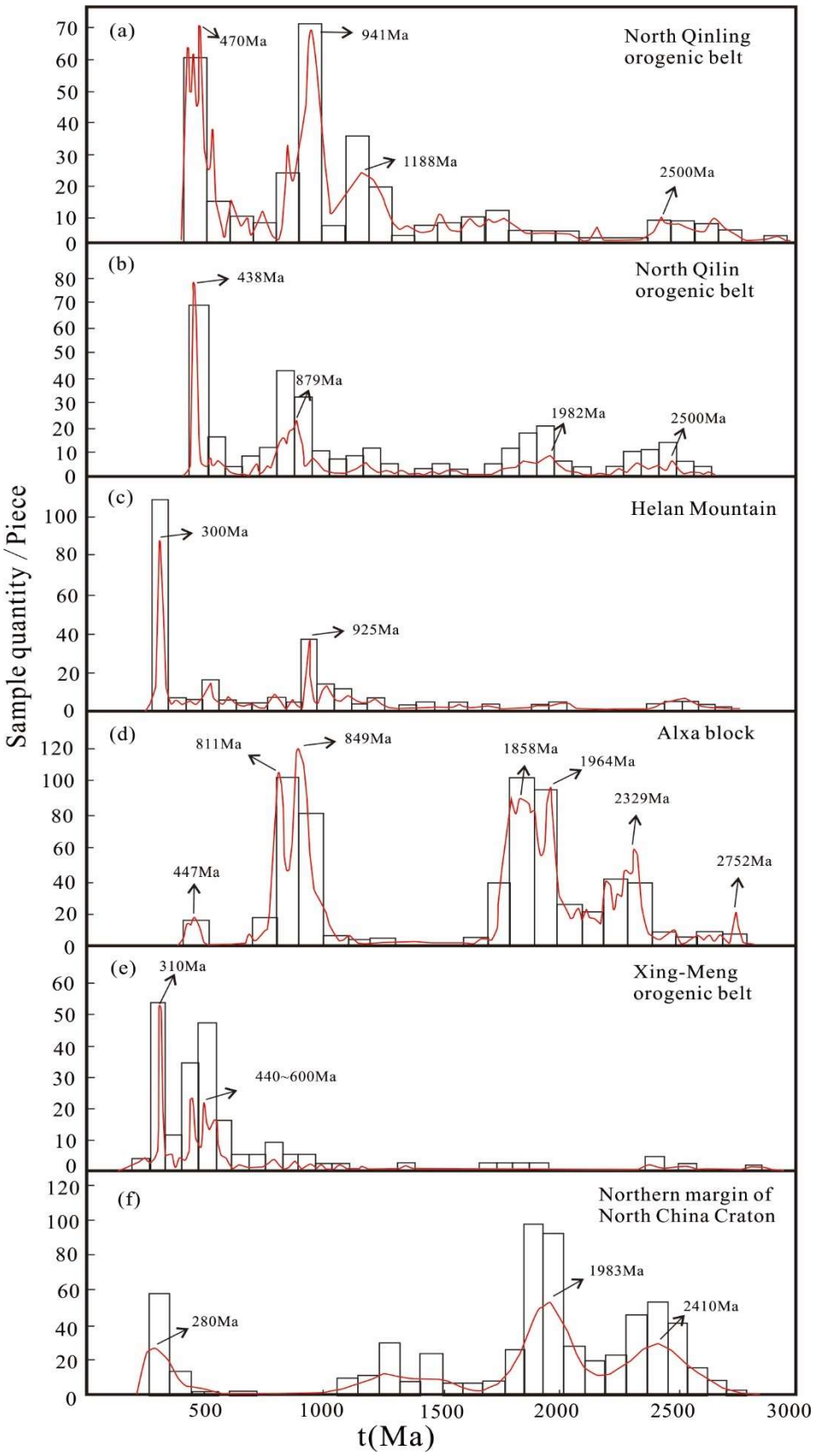

Figure 5. Comparison of U-Pb ages spectra for detrital zircons from the red sandstone in Danxia landform area of Jingbian and rocks of the adjacent potential sources.

 doi:10.20944/preprints202211.0025.v1

5.2. Characteristics of sandstone deposition process and origin change

According to the zircon U-Pb dating results of the red sandstone clasts (Table 1), the upper, middle and lower parts of the study area have certain variation characteristics of deposition. The early origin area is mostly near-origin transport, and the origin area is mainly the North China Massif and the Alashan Massif (Figure 4, Figure 5d, Figure 5f), and the late origin area appears to be distant-origin, namely the Xingmeng orogenic belt (Figure 4, Figure 5e). As reflected from the vertical section, the upper and lower origin areas are mostly near-origin, and the central part has the largest proportion of relative distant origin, and the origin area has the strongest erosion and transport during the upper deposition of red sandstone, stronger fluvial erosion and transport, and longer transport distance; the central deposition period has the smallest erosion and transport, smaller fluvial erosion and transport, and closer transport distance; the lower deposition period has moderate erosion and transport; and the transport distance is moderate.

5.3. Classification of origin systems and paleogeographic characteristics

The origin of the Ordos Basin is considered to be bi-directional from north to south, and the origin of the northern part of the basin is mainly from the Alashan-Yinshan paleosol [56,57], while the origin of the southern part of the basin is mainly from the Qinling-Qilian orogenic belt [58,59], and the different origins also determine the lithological differences of the sandstones. According to the aforementioned, the red sandstones of the Luohe Formation in the study area are located in the central part of the basin, and the origins are mainly from the Xingmeng orogenic belt, the Alashan Massif and the North China Massif. The Qinling-Qilian orogenic belt has less influence on their origins, showing that the origin supply in the central part of the basin was mainly from the north during the deposition period. The internal North China Craton also made important contributions. The origin system in the south was less developed.

On the basis of previous studies, combined with the characteristics of origin changes revealed by field investigations and detrital zircons, it can be linked to the tectonic-movement paleogeographic pattern of the corresponding period in the study area. The early-mid Paleozoic period is the main period of basement formation in the Ordos Basin. Under the influence of several tectonic movements, the basement rock system underwent metamorphism, mixed lithification and folding, and an ancient basement rock system dominated by TTG gneisses and mantle-derived granites was formed in the 2500 Ma period, which finally formed a stable crystalline basement after the Lvliang movement[60]. The interior of the basin is dominated by broad and slow positive magnetic anomalies, showing roughly NE trend, and both sides show negative magnetic anomaly bands with the same trend and large morphological differences[61], and the origin information also shows that there are strong changes in the Jingbian area and large scale magnetic anomaly gradient bands, reflecting the existence of a physical interface in the Ordos basement north of Jingbian. Moreover, the basement material and tectonic features are different on both sides, and the paleogeographic pattern is high in the east and low in the west, high in the north and low in the south, weakly divergent and weakly spreading. During the late Paleozoic-early Miocene, the basin mainly inherited the evolutionary features of the North China plate, and developed continental margin rift valleys and intra-land argillic troughs[61], while the Qinqi Oceanic rift valley and its accompanying argillic troughs were mainly developed on the southern margin of the basin, and the Xingmeng Oceanic rift valley and its accompanying argillic troughs were mainly developed on the northern margin of the basin. The southwest margin faces a vast oceanic basin. With thick sediment and large difference between north and south, the north of the basin is relatively stable due to the persistence of the Yimeng Uplift, and the northeast of the Ordos Massif has become the uplift denudation area. The origin information reveals that the Xingmeng orogenic belt at the north edge of the basin continues to supply a large amount of material to the central part of the basin during this period. During the Late Miocene and Neoproterozoic, the

 doi:10.20944/preprints202211.0025.v1

ancient Asian Ocean subducted to the North China Plate, the north and south margins of the basin were transformed into continental margins and entered the stage of collisional extrusion orogeny. The ocean basins and rift valleys around the basin were closed one after another, and the North China Plate became part of Rodinia supercontinent. During this period, paleogeographic pattern was high in the north and low in the south, with uplift and depression in between. In the middle Paleozoic, due to the influence of the Caledonian movement, the basin generally received uplift and denudation, and the Xingmeng Ocean, Qinqi Ocean and Helan Argentine Trough on the north and south edges of the basin were closed and transformed into an intra-land orogenic belt. In the Late Paleozoic, during the Hexi movement, the basin underwent regional subsidence and began to receive deposition again, and the Qinqi trough, Xingmeng trough, and Helan argillaceous trough were restored, and the origin information shows that the regional tectonics inherited the NNE-oriented uplift and depression interphase pattern in the Early Paleozoic, and the paleogeographic pattern is north-south high and middle low, east-high and west-low, spreading north-south and diverging east-west.

6. Conclusions

(1) The LA-ICP-MS zircon U-Pb dating method was adopted to obtain a total of 182 valid ages in three Cretaceous red sandstone samples from the upper, middle and lower part of the Jingbian Danxia landform area in the central Ordos Basin. The detrital zircon age spectra show that the original material of the red sandstone was formed in three main age intervals (groups), 252-456 Ma (Paleozoic), 1657-2084 Ma (Early Mesozoic-Late Paleozoic), and 2129-2538 Ma (Early-Middle Paleozoic), which record the existence of three main regional tectonothermal events in the origin area, among which the tectonothermal events in the the Mesozoic and Paleozoic are the most active and prominent.

(2) A comprehensive analysis of the clastic zircon U-Pb ages in the three red sandstones concluded that the Xingmeng orogenic belt, the North China Massif and the Alashan Massif were the main origin areas of the Jingbian red sandstones.

(3) Zircon U-Pb age characteristics revealed that the origin area of the Jingbian Red Sandstone was near-origin in the early deposition period and distant in the late deposition period; the vertical profile reflected that the origin area had the strongest erosion and transport in the upper red sandstone deposition period, the smallest erosion and transport in the middle deposition period, and moderate erosion and transport in the lower deposition period.

(4) Analysis of the origin system showed that the origin supply in the central part of the basin was dominated by the northern origin supply during the deposition period, with important contributions from the interior of the North China Craton and a less developed origin system in the south. The origin change characteristics revealed that the paleogeographic pattern is multi-period and cyclic, mainly through four tectonic movement cycles, such as Wutai, Lvliang, Caledon and Haixi. The paleogeographic features of the main periods in the study area were: high in the east and low in the west, high in the north and low in the south, weakly divergent and weakly spreading in the early-middle Paleozoic; high in the north and low in the south, internally divergent, with the sedimentary pattern controlled by the argillic trough in the late Paleozoic-early Miocene; high in the north and low in the south, with uplift and depression in between in the late Miocene-Neogene; high in the north and low in the middle, high in the east and low in the west, spreading north-south and diverging east-west in the Paleozoic.

Author Contributions: Conceptualization, H.S. and D.P.Y.; Data curation, H.S.; Formal analysis, D.P.Y. and J.B.Z.; Investigation, H.S., J.B.Z.,R.L.,X.N.W.,Y.Z. and L.L.; project administration, D.P.Y.; writing-original draft, H.S.; writing-reviewand editing, H.S., D.P.Y. and J.B.Z.. All authors have read and agreed to the published version ofthe manuscript.

Funding: This res was funded by the National Natural Science Foundation of China(41930641) and Development and research project of dynamic monitoring information management system for water and soil conservation of energy development in Shaanxi Province(1204010725)

Acknowledgments: We would like to acknowledge Beijing Gaonian Linghang Technology Co, for their assistance the experiment.

Conflicts of Interest: The authors declare no conflict of interest.

References

1 Peng Hua, Pan Zhixin, Yan Luobin, et al. A review of the research on red beds and Danxialandform[J]. ActaGeographicaSinica, 2013, 68(9):1170-1181.

2 Qi Deli, Yu Rong, Zhang Renshun et al. On the spatial pattern of Danxia landform in China[J]. AtcaGeographicaSinica, 2005,60(1):41-52.

3 Kruiver P P, Dekkers M J, Langereis C G. Secular variation in Permian red beds from Dome de Barrot, SE France[J]. Earth and Planetary Science Letters, 2000,179(1):205-217.

4 Netoff D I, Shroba R R. Conical sandstone landforms cored with clastic pipes in Glen Canyon National Recreation Area, southeastern Utah[J]. Geomorphology, 2001,39(3-4):99-110.

5 Tanner L H, Lucas S G. The Moenave formation: Sedimentologic and stratigraphic context of the Triassic-Jurassic boundary in the Four Corners area, southwestern U.S.A[J]. Palaeogeography, Palaeoclimatology, Palaeoecology, 2007,244(1-4):111-125.

6 Morris T H, Ritter S M, Laycock D P. Geology unfolded: An illustrated guide to the geology of Utah's national parks[M]. Provo: Brigham Young University Press,2010.

7 Peng Xiaohua, Wu Hao, Li Yizhao, et al. A Preliminary Study on the Genetic Mechanism of Wavy Danxia Landform in Longzhou, Jingbian, Shaanxi Province[J]. ActaGeoscienticaSinica,2020,41(03):443-451.

8 Wu Hao, Peng Xiaohua, Zhu Jie, et al. Characteristics and forming environment of wave-type Danxia landform landscape in Longzhou, Jingbian County, Shaanxi Province[J]. Mineral Exploration, 2021,12(02):497-502.

9 Tang Y Z, Xing L D, Li X W, et al. The sedimentary environment of Early Cretaceous dinosaur tracks in Longzhou Danxia landform of Jingbian county, Shaanxi Province[J]. Geological Bulletin of China, 2020,39(4):425-432.

10 Peng Hua. A Survey of the Danxia Landform Research in China[J]. Scientia GeographicaSinica,2000,(3):203-211

11 Pan Zhixin, Ren Fang, Chen Liuqin, er al. Characteristics of Danxia landform in the northern Shaanxi and a comparison with other Danxia areas in and outside China[J]. Scientia GeographicaSinica, 2021,41(6):1069-1078.

12 Fedo C M, Sirocombe K N, Rainbird R H. Detirtal zircon analysis of the sedimentary record[J]. Reviews in Mineralogy and Geochemistry, 2003,53(1):277-303.

13 XU Huan, GUO Fusheng, CHEN Liuqin, et al. LA-ICP-MS Zircon U-Pb Dating of Tuffs in the Taining Basin: Constraints on the Ages of the Danxia Red Beds[J].Acta Geologica Sinica(English Edition),2019,93(06):1976-1977.

14 Wang Y J, Chen L Q, Li W H, et al. Detrital zircon U- Pb dating of the Late Cretaceous aeolian sandstones from the Tangbian Formation in the Yiyang area of Jiangxi Province and its provenance significance. Geological Bulletin of China, 2019, 38(4):667-679.

15 Yang Qingkun, Liu Fujun, Hua chen, et al. Paleoclimate characteristics and provenance analysis of detrital zircons of aeolian sandstone on Jinshiyan section in Danxia formation， Danxia Basin,Guangdong province[J]. Journal of Arid Land Resources and Environment.2020,34(06):73-80.

16 Safonova I , Perfilova A , Obut O, et al. "Traces of intra-oceanic arcs recorded in sandstones of eastern Kazakhstan: implications from U-Pb detrital zircon ages, geochemistry, and Nd-Hf isotopes." International Journal of Earth Sciences (2021):1-20.

17 Shuang LI, Saijun SUN, Xiaoyong YANG, et al. Detrital zircon U-Pb age perspective on the sediment provenance and its geological significance of sandstones in the Lamandau region, SW Borneo, Indonesia[J].Journal of Oceanology and Limnology,2022,40(02):496-514.

 doi:10.20944/preprints202211.0025.v1

18 Weltje G J, Eynatten H V. 2004. Quantitative provenance analysis of sediments: Review and outlook[J]. Sedimentaty Geology, 171: 1−11.

19 Andersen T 2005. Detrital zircons as tracers of sedimentary provenance: Limiting conditions from statistics and numerical simulation[J]. Chemical Geology, 216: 249−270.

20 Wei Bin, Zhao Zhongyi, Yang Youyun. Sedimentary facies of the Cretaceous Luohe and Huanhe-Huachi formations in the Ordos Basin[J]. Journal of Statigraphy, 2006,30(4):367-372.

21 Zhao Zhenyu, GuoYanru, Wang Yan, et al. Study progress in tectonic evolution and paleogeography of Ordos Basin[J]. Special Oil and Gas Reservoirs, 2012,19(5):15-20.

22 Cheng Xianyu, Zhang Tianfu, Miao Peisen, et al. Detrital zircon U-Pb dating from the uranium-bearing sandstone of Lower Cretaceous of Lower Segment of Luohe Formation in Southwestern Ordos Basin and its peripheral lithospheric extension[J]. Geology in China,2020:1-27,[2022-10-30].

23 HouKejun, Li Yanhe, Tian You Rong. In situ U-Pb zircon dating using laser ablation-muliti ion counting-ICP-MS[J]. Mineral Deposits, 2009,20(4):481-492.

24 Ludwig K R. User's manual for Isoplot 3.0: A Geochronological Toolkit for Microsoft Excel[M]. Berkeley Geochronology Center Special Publication, 2003, 4: 1~70.

25 Anderson T.Correction of common lead in U-Pb analyses that do not report204Pb[J] Chemical Geology, 2002, 192 (1/2) :59-79.

26 Jordan T H. Structure and formation of the continental tectosphere[J]. Journal of Petrology, 1988, 29: 11~37

27 Anderson D L. New theory of the earth[M]. Cambridge: Cambridge University Press, 2007: 1~384.

28 Gehrels G, Johnsson M J, Howell D G.Detrital zircon geochronology of the Adamsargillite and Nation River Formation, East-Cen-tral Alaska, U.S.A[J].Journal of Sedimentary Research, 1999, 69:135-144.

29 Sircombe K N.Tracing provenance through the isotope ages of littoral and sedimentarydetrital zircon, eastern Australia[J].Sedimenta-ry Geology, 1999, 124:47-67.

30 Belousova E A, Griffin W L, O'Reilly S Y, Fisher N J.2002. Igneous zircon: Trace element composition as an indicator of source rock type[J]. Mineralogy and Petrology, 143:602-622.

31 Crofu F, Hanchar J M, Hoskin P W O, Kinny P. 2003. Atlas of zircon textures[J]. Reviews in Mineralogy and Geochemistry, 53:469-500.

32 Zhao Hongge, Liu Chiyang, Wang Hairan, et al. 2015. LA-ICP-MS Detrital Zircon Dating and its Provenance Significance in Yan'an Formation of the Early-Middle Jurassic in the Northwestern Margin of Ordos Basin[J]. Earth Science Frontiers, 22(3): 184-193.

33 Ma Shouxian, Meng qingren, Qu Yongqiang. 2011. A study of detrital zircons of Late Carboniferous-Middle Triassic strata in the northern margin of North China block and its geological implication[J]. Geological Bulletin of China, 30(10):1485-1500.

34 Chen Yuelong, Li Dapeng, Wang Zhong, et al.2012.History of formation and evolution on the crust around the Ordos Basin: Evidences from U-Pb dating and Hf isotopic composition of zircons[J]. Earth Science Frontiers, 19(03):147-166.

35 Chen Bin, Zhao Guochun, Simn WILDE. 2001. Subduction and Collision -related Granitoids from Southern Sonidzuoqi, Iner Mongolia: Isotopic Ages and Tectonic Implications[J]. Geological Review , (04):361-367.

36 Zhang, S.H., Zhao, Y., Liu, J, et al., 2007. Emplacement Depths of the Late Paleozoic-Mesozoic Granitoid Intrusions from the Northern North China Block and Their Tectonic Implications[J]. Acta Petrologica Sinica, 23(3): 625-638.

37 Zhai Mingguo.2004.Decomposition of 2.1-1.7Ga geological event group in North China Craton and itstectonic significance[J].Acta Petrologica Sinica,20(6):1343-1356.

38 Dan W, Li X H, Wang Q, et al.2014.Paleoproterozoic S-type granites in the Helanshan Complex, Khondalite Belt, North China Craton: Implications for rapid sediment recycling during slab break-off[J].Precambrian Research,254: 59-72.

39 Xu Huan. 2019. Tectonic magmatism of middle-late Paleoproterozoic in the southwestern Ordos Block[D]. Northwestern University, 1-148

 doi:10.20944/preprints202211.0025.v1

40 Zhang, J. X., Gong, J. H., 2018. Revisiting the Nature and Affinity of the Alxa Block[J]. Acta Petrologica Sinica, 34 (4): 940-962.

41 Li Junjian, Luo Hui, Zhou Hongying, et al.2004.Metallogenic epoch of Zhulazaga gold deposit in Alxa area,Inner Mongolia Autonomous Region[J].Geochimica,33(6):663-669.

42 Zhou Xiwen, Geng Yuansheng.2009.Metamorphic age of the khondalite series in the Helanshan region: evolution of the western block in the North China Craton[J].Acta Petrologica Sinica,25(8):1843-1852.

43 Gong Jianghua, Zhang Xinjian, Yu Shengyao. 2011. The origin of Longshoushan Group and associated rocks in the southern part of the Alxa block: constraint from LA-ICP-MS U-Pb zircon dating[J]. Acta Petrologica et Mineralogica ,30(05):795-818.

44 Yang Pu, Chen Gang, Chen Qiang, et al.2015.U-Pb Dating Of Detrital Zircon from Upper Ordovician Pingliang Formation in Southwest Margin of the Ordos Basin and Provenance Analysis[J].Geological Review,61(1):172-182

45 Song Zhijie, Liu Wencan, Zhang Hongyuan, et al.2019. Detrital zircon geochronology and its geological significance of upper Permian sandstones in Yushigou area of western Qilian Mountains, China[J]. Geoscience,33(01):112-120.

46 Lin Shaoze, Wang Fei, Xie Chenglong, et al.2019.Early Cretaceous Structural Evolution and Formation Model of the Kalaqin Metamorphic Core Complex in the Northern Margin of the North China Craton[J].Geotectonica et Metallogenia,43(1):1-16.

47 Zhai, M.G., Peng, P., 2007. Paleoproterozoic Events in the North China Craton. Acta Petrologica Sinica, 23(11): 2665-2682.

48 Zhai Mingguo. 2011. Cratonization and the Ancient North China Continent:A summary and review[J].Science China(Earth Sciences) ,54(08):1110-1120.

49 Zhai Mingguo. 2013. Secular changes of metallogeme systems link with continental evolving of the North China Craton[J]. Acta Petrologica Sinica,29(5):1759-1773.

50 Tung Kuoan, Yang Huaijen, Yang Houngyi et al. SHRIMP U-Pb geochronology of the zircons from the Precambrian basement of the Qilian Block and its geological significances[J]. Chinese Science Bulletin, 2007, 52(19) : 2687-2701.

51 Wan YS, Liu YB, Dong CY, et al. 2011. SHRIMP zircon dating of meta-sedimentary rock from the Qinling Group in the north of Xixia, North Qinling Orogenic Belt: Constraints on complex histories of source region and timing of deposition and metamorphism[J]. Acta Petrologica Sinica,27(4):1172-1178.

52 Gong Jianghua, Zhang Jianxin, Yu Shengyao, et al. 2012. 2.5Ga TTG rocks in the western Alxa Block and their implications[J]. Science Bulletin, 57(28~29):2715-2728.

53 Zhang Jin, Li Jinyi, Liu Jianfeng, et al.2012.The relationship between the Alxa Block and the North China Plate during the Early Paleozoic:New information from the Middle Ordovician detrial zircon ages in the eastern Alxa Block[J].Acta Petrologica Sinica,28(9):2912-2934.

54 Zou, L., Liu, P.H., Tian, Z.H., et al., 2019. Late Paleozoic Metamorphic Complex of Precambrian Metamorphic Basement from Eastern Alxa Block: New Evidence from Zircon LA-ICP-MS U-Pb Dating of Boluositanmiao Complex[J]. Earth Science, 44(4): 1406-1423.

55 Dong Chunyan, Wan Yusheng, Xu Zhongyuan, et al.2012.Late Neoarchean magamatism identified in Daqingshan,Inner Mongolia:SHRIMP zircon U-Pb dating[J].Acta Petrologica Sinica,31(6):1509-1517.

56 Zhang Chengli, Liu Liang, Wang Tao, et al. 2013.Granitic magmatism related to Early Paleozoic continental collision in North Qinling[J].Chinese Science Bulletin, 58(35): 4405-4410.

57 Xi Shengli, Wang Huaiguang, Qin Boping.2022. Analysis of the material sources of Shanxi Formation and Shihezi Formation in North E'Erduosi Basin[J]. Natural Gas Industry, 22(2): 21-24.

58 Shi Xiaolin, Chen Gang, Yang Fu, et al. 2015. The detrital zircon U-Pb geochronology and its provenance significance of Kongtongshan conglomerate deposits in southwestern Ordos Basin[J]. Geological Journal of China Universities, 21(4): 719-726.

59 Liang Fei, Huang Wenhui, Niu Jun. 2018. Provenance analysis of Permain Shan1 and He 8 formation in Permian in southwest Ordos Basin[J]. Acta Sedimentologica Sinica, 6(1): 142-153.

 doi:10.20944/preprints202211.0025.v1

60 Yang Hua, Xi Shengli, Wei Xinshan, et al. 2006. Evolution and natural gas enrichment of multicycle superimposed basin in Ordos Basin[J]. China Petroleum Exploration, 11(1):17-25.

61 Duan Jiye, Liu Pengju, Xia Derxin. 2002. The preliminary research on tectonic pattern and tectonic evolution of Mesoproterozoic-Paleozoic in North China plate[J]. Geoscience, 16(4): 331-228.